WARWICK
THE UNIVERSITY OF WARWICK

Original citation:
Shestov, S. V., Nakariakov, V. M. (Valery M.), Ulyanov, A. S., Reva, A. A. and Kuzin, S. V..
(2017) Nonlinear evolution of short-wavelength torsional Alfvén waves. The Astrophysical
Journal, 840 (2). 64.

Permanent WRAP URL:
http://wrap.warwick.ac.uk/88284

Published version: http://dx.doi.org/10.3847/1538-4357/aa6c65

warwick.ac.uk/lib-publications

NONLINEAR EVOLUTION OF SHORT-WAVELENGTH TORSIONAL ALFVÉN WAVES

S. V. Shestov[1,2]

Solar-Terrestrial Centre of Excellence — SIDC, Royal Observatory of Belgium, Avenue Circulaire 3, 1180 Brussels, Belgium

V. M. Nakariakov

Centre for Fusion, Space and Astrophysics, Department of Physics, University of Warwick, Coventry CV4 7AL, UK,
St. Petersburg Branch, Special Astrophysical Observatory, Russian Academy of Sciences, 196140, St Petersburg, Russia

A. S. Ulyanov and A. A. Reva and S. V. Kuzin

Lebedev Physical Institute, Leninskii prospekt, 53, 119991, Moscow, Russia

(Dated: Received ..; accepted ...)

[1]Lebedev Physical Institute, Leninskii prospekt, 53, 119991, Moscow, Russia
[2]s.shestov@oma.be

ABSTRACT

We analyse nonlinear evolution of torsional Alfvén waves in a straight magnetic flux tube filled in with a low-β plasma, and surrounded with a plasma of lower density. Such magnetic tubes model, in particular, a segment of a coronal loop or a polar plume. The wavelength is taken comparable to the tube radius. We perform numerical simulation of the wave propagation using ideal magnetohydrodynamics. We find that a torsional wave nonlinearly induces three kinds of compressive flows: the parallel flow at the Alfvén speed, that constitutes a bulk plasma motion along the magnetic field, the tube wave, and also transverse flows in the radial direction, associated with sausage fast magnetoacoustic modes. In addition, nonlinear torsional wave steepens and its propagation speed increases. The latter effect leads to the progressive distortion of torsional wave front, i.e. nonlinear phase mixing. Because of the intrinsic non-uniformity of the torsional wave amplitude across the tube radius, the nonlinear effects are more pronounced in regions with higher wave amplitude. They are always absent at the axes of the flux tube. In the case of a linear radial profile of the wave amplitude, the nonlinear effects are localised in an annulus region near the tube boundary. Thus, the parallel compressive flows driven by torsional Alfvén waves in the solar and stellar coronae, are essentially non-uniform in the perpendicular direction. The presence of additional sinks for the wave energy reduces the efficiency of the nonlinear parallel cascade in torsional Alfvén waves.

Keywords: Sun: corona — Sun: oscillations — magnetohydrodynamics (MHD) — waves

1. INTRODUCTION

The existence of plane Alfvén waves was theoretically predicted by Alfvén (1942), and since then the ubiquitous presence of Alfvén waves was found in magnetospheric, space, cosmic and laboratory plasmas (e.g. Uberoi 1995; Cheng et al. 1985; Chaston et al. 2000). In solar physics Alfvén waves are mainly considered as a candidate for coronal heating due to their ability to freely propagate from lower layers of the solar atmosphere to the corona (e.g. Ruderman 1999; Srivastava et al. 2017). For example, Copil et al. (2008) suggested that propagating Alfvén waves could locally heat coronal plasma threads. In addition, Fletcher & Hudson (2008) proposed that a flare-generated large-scale torsional wave could accelerate electrons to high energies. Alfvén waves may also contribute to the acceleration of the solar and stellar winds (e.g. Charbonneau & MacGregor 1995; Cranmer 2009; Matsumoto & Suzuki 2012), and collimate astrophysical jets (Bisnovatyi-Kogan 2007).

In the presence of field-aligned plasma non-uniformities, typical for the corona, Alfvén waves appear in a form of torsional waves (e.g. Van Doorsselaere et al. 2008). Torsional Alfvén waves are azimuthal (rotational) perturbations of the plasma velocity accompanied by azimuthal components of the magnetic field. Linear torsional waves propagate along the magnetic field at the local Alfvén speed.

The key element of the nonlinear evolution of linearly and elliptically polarised Alfvén waves is the ponderomotive force that is associated with the variation of the abso-

lute value of the magnetic field in the wave (e.g. Hollweg 1971; Tikhonchuk et al. 1995). This variation results in the gradient of the magnetic pressure that induces plasma flows and hence changes the density of the plasma. The induced compressive perturbations have double the frequency of the mother Alfvén wave. The induced variations of the absolute value of the magnetic field and plasma density change the local values of the Alfvén speed, and cause the Alfvén wave self-interaction resulting in steepening of the wave front (e.g. Ofman & Davila 1995; Zheng et al. 2016).

Nonlinear dynamics of Alfvén waves is actively studied analytically and numerically, with the main emphasis put on the study of plane waves. It has been shown that weakly-nonlinear plane Alfvén waves are governed by the Cohen–Kulsrud evolutionary equation that is a modification of the well-known Burgers equation on accounting for the cubic nonlinearity intrinsic to Alfvén waves (e.g. Cohen & Kulsrud 1974). In addition, when the wave front is non-plane or oblique, Alfvén waves induce oblique compressive perturbations (e.g. Malara et al. 1996; Nakariakov et al. 1997). The ponderomotive acceleration effects have been intensively studied in the context of acceleration of the solar and stellar winds (e.g. Ofman & Davila 1998; Nakariakov et al. 2000; Suzuki 2011), and also of the first ionisation potential effect (e.g. Laming 2015).

Nonlinear evolution of plane Alfvén waves is strongly affected by transverse structuring of the plasma in the Alfvén speed and/or field-aligned plasma flows. The transverse structuring of the medium leads to the wavefront distortion, the wave becomes progressively non-planar, and the effect of phase mixing comes into play. It causes enhanced dissipation of Alfvén waves (e.g. Heyvaerts & Priest 1983; Hood et al. 2002), and induces compressive perturbations that produce fast and slow magnetoacoustic waves (e.g. Nakariakov et al. 1997; Nakariakov et al. 1998; Botha et al. 2000; Tsiklauri & Nakariakov 2002; Tsiklauri et al. 2003).

However, in a plane wave the perpendicular scale, i.e. the length of the wave front, should be much larger than the parallel wavelength, which is rarely fulfilled. For example, in the solar corona the generation of a plane Alfvén wave with a 10-min period and the Alfvén speed of $1\,\mathrm{Mm\,s^{-1}}$ the wave driver at the base of the corona should be much larger than 600 Mm (i.e. much larger than the radius of the Sun). As the solar corona is structured into magnetic flux tubes, represented, for example, by coronal loops, plumes and various filaments, coronal Alfvén waves are likely to appear in the form of torsional, rather than plane perturbations. Torsional waves have received attention in the context of heating of the plasma in coronal loops. In particular, Poedts & Boynton (1996); Ruderman et al. (1997) considered dissipation of finite amplitude waves driven periodically at one footpoint of a closed magnetic structure. On the other hand, Antolin & Shibata (2010) established several constraints on the parametric range of Alfvén waves as a coronal heating mechanism.

The understanding of the appearance of coronal Alfvén waves in the torsional form stimulated intensive studies of nonlinear evolution of torsional waves. Kudoh & Shibata (1999) and Vasheghani Farahani et al. (2011) numerically and analytically, respectively, demonstrated that propagating torsional Alfvén waves, similarly to plane waves, induce **compressive** perturbations due to the ponderomotive force associated with nonlinear effects. Vasheghani Farahani et al. (2012) found that weakly-nonlinear self-interaction of torsional Alfvén waves results in the Cohen–Kulsrud steepening of the wave profile, while the coefficients are different from the case of a plane wave. **The self-interaction occurs due to the nonlinear excitation of compressive waves and their back-reaction on the mother torsional waves.** Fedun et al. (2011) showed by means of numerical simulations that chromospheric magnetic flux tubes can act as a frequency filter for torsional waves. **Mikhalyaev & Bembitov (2014) studied analytically the resonant generation of compressive waves by nonlinear coupling of two torsional waves propagating in the opposite directions.** Murawski et al. (2015); Wójcik et al. (2017) highlighted the effect of the expanding magnetic tube on the evolution of torsional Alfvén waves, and emphasised the importance of the stratification. **Williams et al. (2016) modelled the propagation of torsional waves in the presence of slow compressive shocks.**

However, the efficiency of nonlinear interaction of torsional and compressive waves is not understood in detail so far. In particular, the role of the transverse profile of the torsional wave needs to be revealed. The main motivation for this study is the intrinsic non-uniformity of the wavefronts of torsional waves. Indeed, as the finite amplitude effects increase the wave propagation speed (e.g. Cohen & Kulsrud 1974), and as the torsional wave has a zero amplitude at the axis of the guiding magnetic flux tube and increases to the tube boundary, the propagation speed is always non-uniform across the field. It creates the conditions for phase mixing even if the Alfvén speed inside the flux tube is uniform, as the torsional waves have different nonlinear increase in the propagation speed at different distance from the tube axis. This nonlinear phase mixing leads to the generation of compressive perturbations. The induced compressive perturbations may lead to the torsional wave self-interaction. Also, in contrast with the incompressive Alfvén waves, the induced compressive perturbations can be detected with imaging telescopes, and are subject to enhanced damping by various dissipative mechanisms.

The aim of this paper is to study by means of 3D magnetohydrodynamic (MHD) modelling the effects of nonlinear excitation of compressive perturbations by a torsional wave of finite amplitude. We consider the parallel wavelength to be not much larger than the radius of the magnetic flux tube, and thus account for the nonlinear phase mixing. This approach is a finite-wavelength generalisation of the analytical theory developed by Vasheghani Farahani et al. (2011)

in the thin flux tube approximation that corresponds to the long wavelength limit. **We neglect the effect of the stratification of the atmosphere, as the typical radii of coronal field-aligned plasma non-uniformities and hence the considered wavelengths are about 1–10 Mm, while the typical scale heights of the stratification exceed 50 Mm. Thus, we consider evolution of torsional waves in a flux tube that is uniform along its axis.** The paper is organised as follows: in Section 2 we describe our numerical setup, in Section 3 we discuss the results obtained, and finally give conclusions in Section 4. Appendix A illustrates the nonlinear excitation of compressive perturbations by a long-wavelength torsional waves in the thin flux tube approximation, and Appendix B illustrates the generation of compressive waves due to the phase-mixing effect.

2. NUMERICAL SETUP & INITIAL CONDITIONS

2.1. *MHD equations and normalisation*

The simulations were performed using the numerical code MPI-AMRVAC (Porth et al. 2014). The code applies the Eulerian approach to the solution of the resistive MHD equations,

$$\frac{\partial \rho}{\partial t} + \nabla \cdot (\rho \mathbf{v}) = 0, \tag{1}$$

$$\frac{\partial (\rho \mathbf{v})}{\partial t} + \nabla \cdot (\mathbf{v}\rho\mathbf{v} - \mathbf{BB}) + \nabla p_{\text{tot}} = 0, \tag{2}$$

$$\frac{\partial \mathbf{B}}{\partial t} + \nabla \cdot (\mathbf{v}\mathbf{B} - \mathbf{B}\mathbf{v}) = -\nabla \times (\eta \mathbf{J}), \tag{3}$$

$$\frac{\partial e}{\partial t} + \nabla \cdot (\mathbf{v}e - \mathbf{BB} \cdot \mathbf{v} + \mathbf{v}p_{\text{tot}}) = \nabla \cdot (\mathbf{B} \times \eta \mathbf{J}), \tag{4}$$

where e, ρ, $\mathbf{v}$, $\mathbf{B}$ are the total energy density, mass density, velocity, and magnetic field, $p = (\gamma - 1)(e - \rho v^2/2 - B^2/2)$ is the thermal pressure, $p_{\text{tot}} = p + B^2/2$ is the total pressure, $\mathbf{J} = \nabla \times \mathbf{B}$ is the electric current density; η is the electrical resistivity, and γ is the ratio of specific heats. As in this study we are not interested in dissipative processes, we take $\gamma = 5/3$, and $\eta = 0$.

The physical quantities were normalised with the use of the following constants: the lengths are normalised to $L_{\text{N}} = 1$ Mm, magnetic fields to $B_{\text{N}} = 20$ G and densities to $\rho_{\text{N}} = 1.67 \times 10^{-15}$ g cm^{-3}. The mass density normalisation corresponds to the electron concentration $n_{\text{N}} = 10^9$ cm^{-3}. The normalising speed was calculated in the units of $v_{\text{N}} = B_{\text{N}}/\sqrt{4\pi\rho_N} = 1{,}380$ km s^{-1} that is the Alfvén speed corresponding to the values of B_{N} and ρ_{N}, the normalising time was set to $t_{\text{N}} = L_{\text{N}}/v_{\text{N}} = 0.7246$ s, the normalisation of the radial derivative of the azimuthal velocity was set to $\Omega_{\text{N}} = v_{\text{N}}/L_{\text{N}} = 1.38$ s^{-1}. **The values used for the normalisation are typical for the solar corona; their use justifies our intention to analyse nonlinear effects in the coronal plasma.** Further in the text we imply normalised units if it is not stated otherwise.

2.2. *Numerical setup*

We used a cylindrical frame of reference, and considered a straight magnetic tube directed along the z-axis of the computational box. The equilibrium magnetic field is parallel to the tube axis. The equilibrium concentration of electrons, $n_e(r)$ was set using the generalised symmetric Epstein function (Cooper et al. 2003), and the equilibrium parallel magnetic field $B_z(r)$ was set to equalise the equilibrium total pressure everywhere in the computational box,

$$\begin{cases} n_{\text{e}}(r) = n_\infty + \dfrac{(n_0 - n_\infty)}{\cosh^2\left[(r/R_0)^\alpha\right]} \\[2ex] B_z(r) = B_0 \left\{ 1 + \dfrac{4T(n_0 - n_\infty)}{B_0^2} \left(1 - \dfrac{1}{\cosh^2\left[(r/R_0)^\alpha\right]} \right) \right\}^{1/2}, \end{cases} \tag{5}$$

where $R_0 = 1$ is the tube radius, $n_\infty = 0.2$, $n_0 = 1$, $B_0 = 1$, and the temperature T is constant throughout the whole volume. **In physical units these values correspond to $R_0 = 1$ Mm, $n_\infty = 2\times10^8$ cm^{-3}, $n_0 = 10^9$ cm^{-3} and $B_0 = 20$ G, i.e. typical for the corona.** The parameter α controls the tube boundary steepness. We used $\alpha = 36$ that results in a rather sharp boundary. The radial profiles of the electron density $n_e(r)$ and magnetic field $B_z(r)$ are depicted in Figure 1.
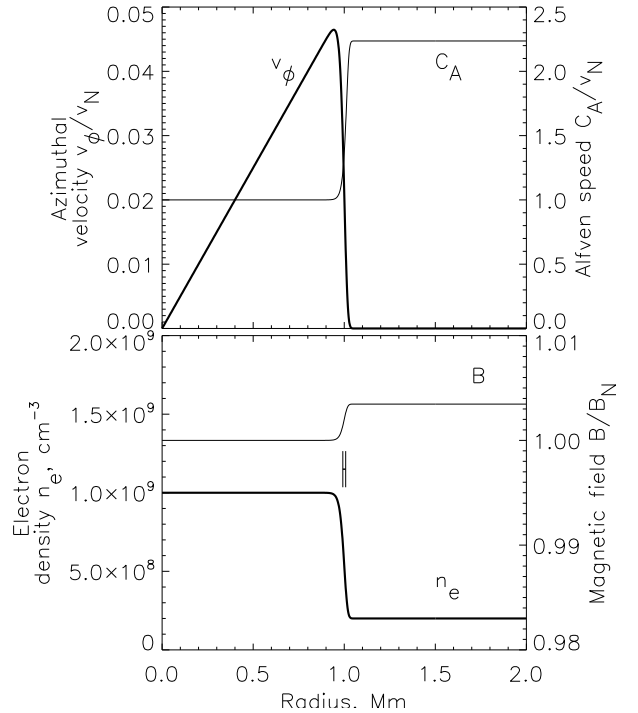
Figure 1. Top: Radial profiles of the normalised initial azimuthal velocity $v_\varphi(r)$ and equilibrium Alfvén speed $C_A(r)$ in the simulated magnetic flux tube. Bottom: Radial profiles of the normalised equilibrium electron density $n_e(r)$ and equilibrium magnetic field $B_z(r)$. The line segment at the point $(1.0, 10^9)$ in the bottom panel indicates the scale of a single pixel used during the simulation.

All the equilibrium values are constant along the z-axis,

Table 1. Parameters of the simulations: the plasma temperature T, wavelength λ, the initial amplitude of the radial derivative of the azimuthal velocity perturbation Ω_M (normalised), and the plasma parameter β.

Title	T, MK	λ, Mm	Ω_M	Plasma β
setup1	0.2	5.0	0.05	0.0035
setup2	0.2	10.0	0.05	0.0035
setup3	1.0	2.0	0.05	0.0173
setup4	1.0	5.0	0.05	0.0173
setup5	1.0	10.0	0.05	0.0173
setup6	1.0	10.0	0.075	0.0173
setup7	1.0	10.0	0.10	0.0173
setup8	1.0	10.0	0.15	0.0173
setup9	1.0	10.0	0.20	0.0173
setup10	5.0	10.0	0.05	0.087

since in this study we consider neither gravity nor transition region.

The torsional Alfvén wave is driven at the bottom wall $z = z_{\min} = 0$ of the equilibrium magnetic flux tube by the following perturbations,

$$B_\varphi(r) = J_M r \frac{\sin(\omega t)}{\cosh^2\left[(r/R_0)^\alpha\right]},$$
$$v_\varphi(r) = \Omega_M r \frac{\sin(\omega t)}{\cosh^2\left[(r/R_0)^\alpha\right]}, \qquad (6)$$

where J_M is the amplitude of the radial derivative of the azimuthal component of the magnetic field, $\Omega_M = -J_M/\sqrt{4\pi\rho(r)}$ is the amplitude of the radial derivative of the azimuthal component of the velocity, and the factor $\cosh^{-2}\left[(r/R_0)^\alpha\right]$ is introduced to avoid the excitation of the torsional wave outside the tube. The frequency ω is set to $\omega = \omega_A = 2\pi/\lambda C_A$, where λ is a wavelength. The top boundary is set to keeps zero gradients of the variables (**the** cont **flag in MPI-AMRVAC). In this study we consider the waves before they reach the top boundary, and hence the specific choice of the top boundary condition is not important.**

2.3. *Parameters of numerical experiments*

We analysed dynamics of the torsional Alfvén wave, controlling the following parameters: the plasma temperature T (and hence, for the fixed value of B_0, on the plasma parameter β that is the ratio of the gas and magnetic pressures), amplitude of the derivative of the azimuthal velocity perturbation, Ω_M, and wavelength λ. The specific values of these parameters in various numerical runs are shown in Table 1.

In all these setups the relative variation of the magnetic field is small, and the plasma-β is less than unity everywhere.

The simulations were performed in a cylindrical frame of reference, in either a 3D (r, φ, z) or 2D (r, z) computational boxes. We used a 3D computational box for the investigation of the general picture of the wave propagation, and high-

resolution 2D computational boxes were used for the analysis of wave-steepening, radial profiles and generation of sausage waves.

In the 3D case the box size was $128 \times 64 \times 256$ grid points, which corresponds to the physical volume $[0, 2]$ Mm in r, $[0, 2\pi]$ in φ, and $[0, 40]$ Mm in z. The numerical grid (pixel) size corresponds to 0.0156 Mm in r (see Figure 1) and 0.156 Mm in z, i.e. much less than the characteristic scales of the non-uniformity and wavelength. In order to test the undesirable effect of the grid resolution we carried out a test run with double the spatial resolution. We found that in both the cases the evolution of the torsional wave shows similar behaviour, in general, but the setup with the lower spatial resolution demonstrated faster decay and a smoother wave profile at the tube boundary.

In 2D simulations we used different grids. For the investigation of wave steepening we used the numerical grid 384×2048, with $r \in [0, 3]$ Mm and $z \in [0, 80]$ Mm, respectively. For the investigation of the radial profiles of the perturbations we used the numerical grid 1024×256, with $r \in [0, 2]$ Mm and $z \in [0, 20]$ Mm, respectively, and for the investigation of sausage magnetoacoustic wave generation we used the grid 384×8192, with $r \in [0, 3]$ Mm and $z \in [0, 320]$ Mm. In all the cases the spatial resolution in the "important" dimension was much higher than in the 3D setup.

In MPI-AMRVAC we choose either HLLC (for 3D simulations), or ssprk54 (for 2D simulations) discretisation method, with the vanleer slope limiter. The constraint $\nabla B = 0$ is controlled by the powel approach. Since we already analysed the effect of numerical resolution on the results, we use no mesh refinement and set the parameter mxnest to 1.

3. RESULTS AND DISCUSSION

3.1. *General picture of torsional wave propagation*

In general, results of the simulation agree with the theory highlighted in Appendix A. A torsional wave appears as an alternate perturbation of the azimuthal plasma velocity accompanied by a perturbation of azimuthal component of the magnetic field, B_φ. The wave dynamics preserves the axial symmetry. Snapshots demonstrating perturbations of various physical quantities in the wave are shown in Figure 2. The wave is seen to propagate along the flux tube, in the positive z-direction, at the speed about the Alfvén speed C_A in the body of the flux tube. At the time of the snapshots $t_1 = 15 t_N = 10.9$ s, the wave has propagated the distance $l_1 = C_A t_1 \approx 15$ Mm $= 1.5\lambda$ from the point of the excitation, $z = 0$.

The local Alfvén speed (see Figure 1) increases near the tube boundary, in a thin layer where the equilibrium plasma density decreases. This leads to the outrunning of the torsional wave near the tube boundaries, producing a distortion

of the wave fronts. It is a clear signature of phase mixing caused by the transverse non-uniformity of the Alfvén speed. **We refer to the effect as linear phase mixing and will further consider it in Section 3.7.**

The detected torsional wave induces flows with two other velocity components, the radial velocity v_r and parallel velocity v_z, and also the density perturbations that propagate at the Alfvén speed and have double the frequency of the driver and the perturbations of the azimuthal velocity v_φ and magnetic field B_φ. **The amplitudes of induced v_r and v_z amounts to square of the amplitude v_φ of the initial wave.**

In addition, in the bottom part of the computational domain (Figure 2) one can see the development of the tube wave propagating at the tube speed $C_T \approx 0.15$ Mm/s. At the time of the snapshot, the wave has propagated the distance $l_2 = C_T t_1 \approx 1.6$ Mm from the excitation point, **which is consistent with Eq. (A19). The tube wave is excited when the plasma temperature is finite, and hence the tube speed C_T is greater than zero.**

The appearance of the parallel compressive perturbations characterised by ρ and v_z may be attributed to the effect of the nonlinear ponderomotive force associated with the gradients of the perturbed Alfvén speed in the parallel direction, and that is in agreement with the theory developed in Vasheghani Farahani et al. (2011), see also Eq. (A18). The excitation of the radial flows that are compressive too, may be attributed to the nonlinear ponderomotive force associated with the gradients of the perturbed Alfvén speed in the perpendicular direction (Nakariakov et al. 1997), see also Appendix B, and to the effect of nonlinear phase mixing, connected with the radial non-uniformity of the torsional wave amplitude.

3.2. *Radial profiles of induced compressive perturbations*

The radial structure of the induced parallel flows at the speed v_z, obtained in the simulation (see Figure 3) is seen to be different from that described by expressions (A1) and (A20) obtained in the thin flux tube approximation. It clearly shows a parabolic shape, $\propto r^2$. This **difference** could be attributed to the finite wavelength effects. A similar radial dependence is seen in the radial structure of the perturbed parallel magnetic field B_z (not shown here).

The simulated radial profile of v_z was found to be well fitted with an almost parabolic dependency,

$$v_z(r,z,t) = \frac{\Omega_M^2 r^2}{4 C_A} \frac{(1 - \cos[2\omega(t - z/C_A)])}{\cosh^4[(r/R_0)^{36}]}, \quad (7)$$

determined empirically, by a guess. The radial dependence in the denominator is **artificially** used to reproduce the disappearance of the perturbation at the flux tube boundary. This parabolic dependence is different from the solution for u_p, given by Eq. (A20) that is independent of the radial coordinate r. **We need to emphasise that the dependence given by Eq. (7) is fully empirical, and is not based on any theoretical result. It is shown here for its possible usefulness**

for forward modelling of the observational manifestation of this effect, when it would be convenient to have a single functional expression for the radial structure of the induced parallel flows. The perturbations of the density ρ and pressure p do not show dependence on the radial coordinate, and have a constant amplitude across the flux tube.

The radial profiles of v_r and B_r are different from the other variables. They have half the wavelength of the mother torsional wave (given by the perturbations of v_φ and B_φ), and are shifted by $+\pi/4$ relative to the mother torsional wave. The radial structure of v_r can be expressed using the odd terms of the Taylor expansion (see Figure 3), beginning with the linear one that is prescribed by the boundary condition at the loop axis (see also the discussion in Zhugzhda 1996). In the performed numerical run, we found that the radial dependence of the radial velocity inside the flux tube could be best-fitted by the expression $v_r(r) = 0.33r(r^2 - 0.28)$. We note that the radial velocity has relatively large values outside the tube's boundary, whereas the azimuthal and parallel velocities do not penetrate into the external medium.

3.3. *Parallel spatial structure of induced compressive perturbations*

Parallel spatial profiles of the velocities v_r, v_φ, v_z measured **along the z-axis at $r_1 = 0.75$ Mm are shown** in Figure 4. **The profiles are rescaled for the purpose of visualization: v_φ is divided by $\Omega_M r_1 = 3.75 \times 10^{-2}$, and v_r and v_z are divided by $\Omega_M^2 r_1^2/4 C_A = 3.52^{-4}$. This rescaling corresponds to omitting of amplitudes and radial dependencies of the variables in Eqs. (6) and (7) (and with the caveat in Eqs. (A19) and (A20)).** These profiles are consistent with the theory described in Appendix A: the wavelength of the induced parallel flows is a half of the wavelength of the torsional wave, the induced parallel flows have a positive average value, and the amplitude corresponds to one given by Eq. (A18), **i.e. the amplitude of induced parallel velocities is proportional to squared amplitude of the azimuthal perturbation.**

The positive average value of the parallel velocity means a field-aligned bulk plasma flow (e.g., see Ofman & Davila 1998), which can be referred to as the "Alfvénic wind". The wind is produced by the ponderomotive force. However, the wind is canceled on the arrival of the slow, tube wave u_T. A similar effect has been studied in detail in the case of plane Alfvén waves by McLaughlin et al. (2011).

In addition, we see small amplitude perturbations of v_r. **The amplitude of this perturbation is approximately 5 times smaller than the amplitude of parallel motions, and the speed of propagation in the z direction is higher than the speed of the torsional wave.** These perturbations correspond to the third kind of the induced compressive perturbations, the fast magnetoacoustic sausage wave (e.g. Edwin & Roberts 1983; Nakariakov et al. 2012; Yu et al. 2016). In the low-β plasma considered here, this mode is characterised
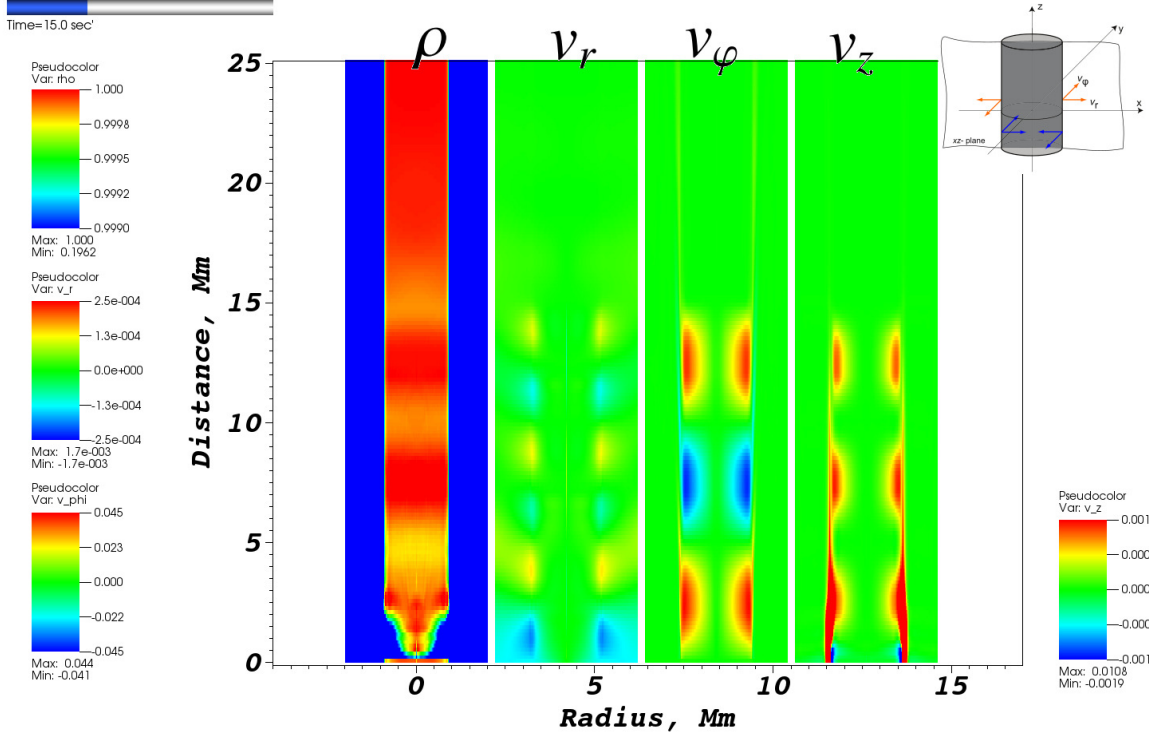
Figure 2. Torsional Alfvén wave propagating along the magnetic flux tube. The panels show the spatial structure of the plasma density ρ and velocities v_r, v_φ, v_z (from left to right) in the xz cross-section through the axis of the flux tube, shown in the inlet. The torsional Alfvén wave is excited at $z = 0$, and propagates in the positive z-direction (upwards). The snapshot corresponds to setup 5, i.e. $T = 1$ MK, $\lambda = 10$ Mm, $\Omega_{\mathrm{M}} = 0.05$; the time instant is $t = 15t_{\mathrm{N}} = 10.9$ s. A relevant animation is available in the online version.
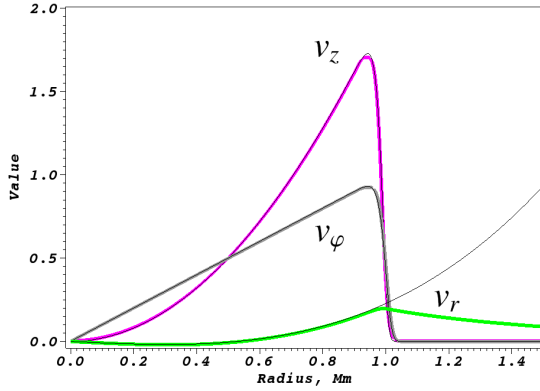

Figure 3. Radial profiles of v_r, v_φ and v_z velocities in the wave maximum. Thick curves are the results of numerical simulation: the black line shows the azimuthal velocity v_φ, magenta curve shows the parallel velocity v_z, and green curve the radial velocity v_r. The profiles are rescaled for the purpose of visualisation: v_φ is divided by $\Omega_{\mathrm{M}} = 0.05$, and v_z and v_r are divided by 6.25×10^{-4}. The thin curves indicate the best-fitting analytical dependencies.

plasma.

Figure 4. Spatial profiles of v_r, v_φ, v_z velocities measured along the z-axis at $r_1 = 0.75$ Mm at the time instant $t = 30\ t_N$. The black curve shows the azimuthal velocity v_φ, the magenta curve the parallel velocity v_z, and the green curve the radial velocity v_r. The profiles are rescaled for the purpose of visualisation: v_φ is divided by $\Omega_{\mathrm{M}} r_1 = 3.75 \times 10^{-2}$, and v_r and v_z are divided by 3.52×10^{-4}.

by compressive, mainly radial flows, and propagates at the speed that lies between the Alfvén speed inside and outside the tube. Positive and negative half-periods of these perturbations are symmetric. Hence, in contrast with the induced parallel flows, they do not constitute any bulk flow of the
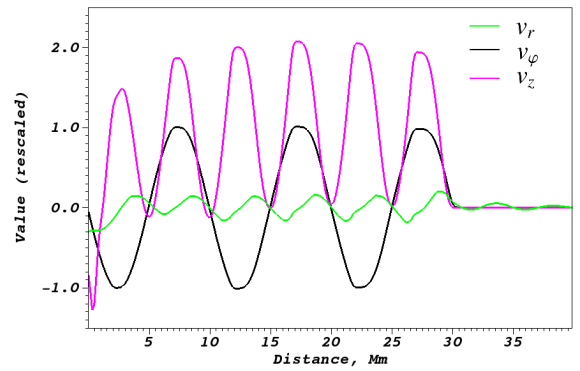
3.4. *Efficiency of the generation of compressive perturbations*

To study whether the efficiency of the nonlinear generation of compressive perturbations depends on various parameters of the plasma, such as the temperature T, wavelength λ and the tube's radius, i.e. to check the validity of the approximation given by Eq. (A20), we perform a parametric study summarised in Table 1.

We analysed amplitudes of the parallel velocity perturbations, v_z, in the leading cycle of the induced wave, at the distance of 10–15 Mm from the origin in Figure 2. According to Eq. (A20), the behaviour of the induced ponderomotive wave depends neither on the temperature T, nor on the wavelength λ. For the amplitude of the ponderomotive wave, numerical setups with different plasma temperatures T **and wavelength λ were found to show good agreement with Eq. (A20) near the boundary of the flux tube.** In addition, we saw the tube wave propagating at the tube speed, which is consistent with Eq. (A19), **again, near the boundary**.

3.5. *Nonlinear wave steepening*

The ponderomotive excitation of compressive flows by an Alfvén wave, leads to the modification of the local Alfvén speed, which, in turn, affects the Alfvén wave itself. This chain of events is considered as nonlinear self-interaction of the Alfvén wave, which leads to the wave steepening (e.g. Cohen & Kulsrud 1974). In the long wavelength limit, steepening of a torsional wave due to nonlinear self-interaction has been considered by Vasheghani Farahani et al. (2012). In that study it was found that the torsional wave steeping occurs at the rate that is lower than in the case of plane Alfvén waves. The **difference** between the evolution of the torsional and plane waves disappears in the case of the cold ($\beta = 0$) plasma. In our work we consider this effect on torsional waves of finite wavelength. For comparison, we modelled nonlinear evolution of a plane Alfvén wave numerically in a 2D Cartesian geometry, and compared it with the results obtained for a torsional wave in the cylindrical geometry. Snapshots of the parallel, along the equilibrium field, structure of the steepened torsional and plane waves of the same amplitudes and wavelengths are shown in Figure 5.

The spatial profiles of both torsional and plane Alfvén waves clearly show the steepening: in the extremes, the perturbations in both the waves overtake the harmonic dependence. It occurs in both positive and negative extremes, which is a typical signature of the nonlinear evolution of linearly or elliptically polarised Alfvén waves (e.g. Cohen & Kulsrud 1974; Vasheghani Farahani et al. 2012). In the case of plane Alfvén waves this effect is seen to be more pronounced, which is consistent with the results obtained by Vasheghani Farahani et al. (2012). But, in contrast to the long-wavelength limit, the decrease in the nonlinear steepening of the finite-wavelength torsional waves occurs even in the case of low-β. It can be attributed to the presence of other sinks of energy, such as the excitation of the sausage mode.
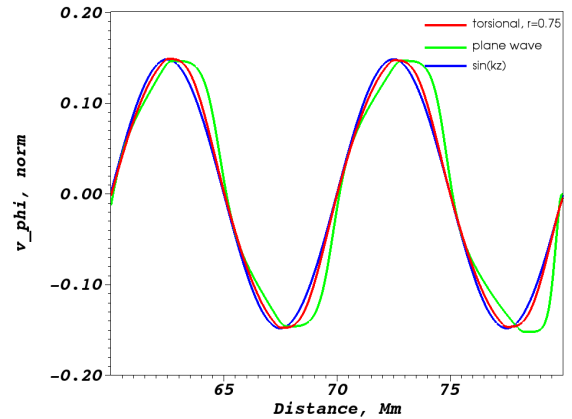

Figure 5. Comparison of snapshots of the azimuthal velocity v_φ in a torsional wave (red) and perpendicular velocity in a plane Alfvén wave (green) of the same relative amplitude. The blue line shows a harmonic function that corresponds to the linear case. Both waves have propagated the distance of $8\lambda = 80$ Mm from the point of the excitation. The amplitude of the torsional wave is measured at 0.75 Mm from the tube axis.

3.6. *Excitation of a sausage wave*

The radial velocities v_r, that were nonlinearly generated by the torsional wave, have an axisymmetric structure, i.e. are independent of the azimuthal coordinate. In a low-β plasma, this spatial structure is similar to the structure of sausage ("$m = 0$") magnetoacoustic modes of the magnetic flux tube, which is an essentially compressive perturbation of the tube. **Sausage modes are collective perturbations of the flux tube, and fill in the whole flux tube. Their specific properties, such as the radial structure and dispersion, are prescribed by the specific radial profile of the fast speed (e.g. Nakariakov et al. 2012; Yu et al. 2016). Consideration of this effect is out of scope of this paper.**

In a low-β plasma, a fast sausage mode propagates at the phase speed v_{saus} that is lower than Alfvén speed of external media $C_A^{\mathrm{ext}} = C_A(r \rightarrow \infty)$, but higher than the Alfvén speed of plasma near the tube's axis, C_A (Edwin & Roberts 1983). As fast sausage modes are highly dispersive, a broadband pulse develops in a sausage wave train. For example, Shestov et al. (2015) numerically studied the dispersive evolution of fast sausage wave trains guided by a magnetic flux tube, and confirmed the formation of wave trains with pronounced modulation of the instant period and amplitude. Also it was found that the propagation speed is higher than the local Alfvén speed in the flux tube, and hence of the torsional wave. Thus, the nonlinearly induced fast sausage wave should propagate faster than the mother torsional wave.

Figure 6 shows the spatial structure of the incompressive and compressive perturbations in the vicinity of the leading front of the torsional wave, with the clear evidence of the fast sausage wave characterised by the perturbations of the density ρ and radial flows v_r preceding the torsional wave

demonstrated by the perturbations of v_φ and the ponderomotively induced parallel flows v_z. The sausage perturbations are seen to propagate at the speed $v_{\text{saus}} \approx 1.3 C_A$, which is consistent with the theoretical estimation of Edwin & Roberts (1983). The amplitude modulation of the sausage wave is also evident. Its amplitude varies in the z-direction, and, in particular, has a maximum at $z \approx 280$ Mm at the instant of time of the snapshot shown in Figure 6.
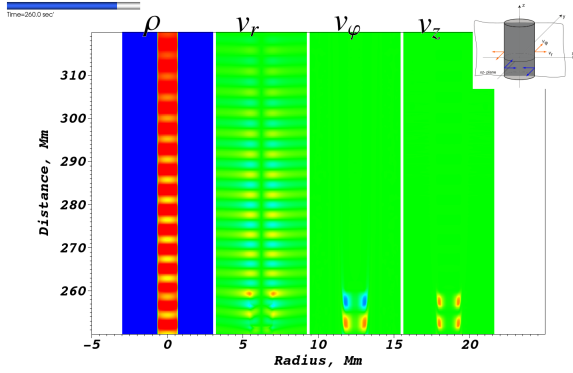

Figure 6. Spatial structure of perturbations in the vicinity of the leading front of the torsional wave, at the distance of 26λ from the excitation point, at the time instant $t = 260 t_N = 188$ s.

3.7. *Linear and nonlinear phase mixing*

The effect of linear phase mixing occurs near the tube boundary, where the local Alfvén speed gradually increases due to the decrease in the plasma density. The efficiency of phase mixing can be estimated using the following kinematic reasoning. The difference δ between the distance travelled by the torsional perturbation near the boundary and in the body of the tube equals to the product of the difference of the local Alfvén speeds at these radial surfaces, ΔC_A and the travel time t. Thus the travel time required for phase mixing of one wavelength $\delta = \lambda$ is the ratio of the wavelength in the body of the tube and the speed difference $t = \lambda / \Delta C_A$. The travel time equals to the distance travelled by the wave from the source, divided by the Alfvén speed in the body of the tube $t = z / C_A$. Thus, the distance at which phase mixing reaches one wavelength equals to $z = \lambda C_A / \Delta C_A$. In particular, in the numerical setup shown in Figure 1, the local Alfvén speed increases near the boundary by about $\Delta C_A \approx 1.2 C_A$, hence for the wavelength of 10 Mm the phase mixing reaches the wavelength at the distance of about 8.3 Mm from the wave source. This value is consistent with the deformation of the torsional wave front seen in the left panel of Figure 7.

Comparing the shapes of the torsional perturbations taken at different distances from the source in Figure 7, we see that at large distances from the source, the perturbation shape experiences some deformation even in the body of the flux tube. More specifically, near the source (left panel), the wave front is clearly deformed because of the non-uniformity of the local Alfvén speed in the region $r > 0.95$ Mm. At $r < 0.95$ Mm, near the source the wave fronts are symmetric with respect to the parallel coordinate. On the other hand, at the larger distance from the source (right panel), the wave front becomes clearly deformed even at the radial distances of $r < 0.8$ Mm. This deformation has the typical signature of phase mixing: the perturbations at larger radial distance from the axis propagate slightly faster. However, at these radial locations the relative change of the local Alfvén speed is negligible. Thus, this phase mixing is not connected with the non-uniformity of the local Alfvén speed. The wave front deformation should be attributed to the variation of the propagation speed of the torsional wave caused by the variation of its amplitude with the radial coordinate. As the torsional wave amplitude increases in the radial direction, it causes additional radial non-uniformity of the torsional wave speed because of the nonlinear acceleration. It can further enhance phase mixing of torsional waves — the effect we shall refer to as "nonlinear phase mixing". In the right panel the torsional perturbation is absent from the region $r > 0.8$ Mm, because of the numerical dissipation of the very strong phase mixing occurring in this region at much shorter distances from the source.

Following the reasoning used in the case of linear phase mixing, the distance at which nonlinear phase mixing reaches one wavelength equals to the product of the wavelength and the ratio of the local Alfvén speed and the increase in the speed caused by the nonlinearity, $z = \lambda C_A / \Delta C_A^{\text{nl}}$, where ΔC_A^{nl} is the difference in the local propagation speeds between the nonlinear and linear torsional waves. The increase in the local speed of the torsional wave, ΔC_A^{nl}, is proportional to the product of the local Alfvén speed and the square of its relative amplitude (see the second term in the brackets on the right hand side of Eq. (22) of Vasheghani Farahani et al. (2012)). As in the performed simulation the relative amplitude of the torsional wave amplitude was 0.05, the effect of nonlinear phase mixing should be rather weak. More specifically, in this run the efficiency of nonlinear phase mixing more than a hundred of times (0.05^2) weaker than of the linear phase mixing that operates near the boundary. Indeed, according to Figure 7, at the distance of about 30 wavelengths from the source, phase mixing equals to a fraction of the wavelength.

4. CONCLUSIONS

We performed numerical simulations of axisymmetric finite-amplitude torsional Alfvén waves in a field-aligned magnetic flux tube filled in with a low-β plasma. The flux tube is straight, untwisted and non-rotating. The flux tube is surrounded by a plasma with the magnetic field directed
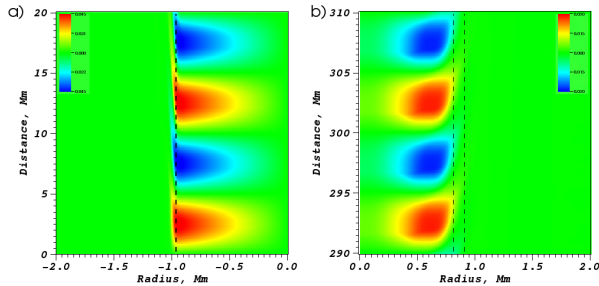
Figure 7. **Comparison of linear and nonlinear phase mixing in a torsional Alfvén wave with the relative amplitude 0.05. Left: snapshot of the azimuthal velocity in the torsional wave that travelled 20 Mm from the source. Right: the same but at the distance of 310 Mm from the source. The vertical dashed lines highlight the radial distances discussed in the text.**

in the same direction as inside the tube, in the direction of the tube axis. The plasma density inside the flux tube is enhanced, which makes the tube a fast magnetoacoustic waveguide. The plasma parameter β is taken to be small everywhere. The torsional perturbations are excited at one footpoint of the tube as alternate periodic azimuthal rotations of the tube. The wavelength of the driven torsional wave is of the same order as the diameter of the flux tube. In the linear regime, the torsional wave is incompressive and consists of the alternate azimuthal flows and the perturbations of the azimuthal component of the magnetic field.

We found that nonlinear evolution of the torsional Alfvén wave leads to the excitation of three different kinds of compressive motions that propagate along the axis of the magnetic flux tube: the well-known parallel flow of the plasma at the Alfvén speed; another parallel flow, at the tube speed, that is the slow magnetoacoustic wave; and, in addition, the mainly radial axisymmetric perturbations propagating at the speed higher than the Alfvén speed inside the flux tube, i.e. faster than the speed of the mother torsional waves. The latter kind of induced waves is the sausage fast magnetoacoustic modes. The sausage mode perturbs the plasma also outside the flux tube, which is consistent with the radial structure of sausage modes. Nonlinearly induced flows of all three kinds have double the frequency of the mother torsional wave.

The nonlinearly induced parallel plasma flow that propagates at the Alfvén speed can be considered as the "Alfvénic wind", as its average over the oscillation period is not zero. The Alfvénic wind is absent from the vicinity of the flux tube axis, where the torsional wave amplitude is always zero. Thus, the parallel plasma flow that is nonlinearly induced by a torsional Alfvén wave has an annulus shape. **The effect of Alfvénic wind has been concluded to be a possible mechanism for the acceleration of solar and stellar winds (e.g.** Ofman & Davila 1998**;** Suzuki 2011**), but those estimations were based on the assumption of plane Alfvén waves.** Our study demonstrates that the field-aligned com-

pressive flows induced by Alfvén waves in the solar and stellar coronae are essentially non-uniform in the transverse (e.g., the horizontal direction in the case of open magnetic configurations in coronal holes). There are always regions that are situated near the axes of the wave-guiding magnetic flux tubes, where the Alfvénic winds are zero. It may have important implications for the solar and stellar wind acceleration problems, **which require a dedicated study**.

The intrinsic radial non-uniformity of the torsional wave amplitude, which is connected with the need to satisfy the zero boundary condition at the axis of the flux tube, leads to the effect of nonlinear phase mixing. This effect is connected with the nonlinear increase in the wave speed at the radial shells where the wave amplitude is higher. It leads to the additional distortion of the torsional wave front and hence the generation of progressively small scales in the radial direction. In particular, this effect should enhance the nonlinear generation of the sausage modes. For example, for a simple, linearly growing in the radial direction radial profile of the torsional wave amplitude, the wave front propagates faster near the flux tube boundary because of the nonlinear effects. Thus, phase mixing occurs even if the radial profile of the Alfvén wave is flat, when this effect is absent for linear Alfvén waves. **Further investigation of this effect would be of interest.**

The induced compressive flows modify the local Alfvén speed, causing the self-interaction of torsional Alfvén waves. It causes the wave profile steepening that is a signature of the nonlinear cascade along the field. The comparison of the nonlinear steepening of the torsional wave with this effect in a plane Alfvén wave of the same amplitude and wavelength showed that the efficiency of the parallel nonlinear cascade in a torsional wave is lower than in a plane Alfvén wave. It could be attributed to the presence of additional sinks for the torsional wave energy, for example, the excitation of the sausage wave. The steepening takes place at some radial distance from the flux tube axis, and is strongest where the torsional wave amplitude is highest, e.g. near the flux tube boundary in the case of a linear radial profile of the torsional wave amplitude.

For the linear profile of the torsional wave amplitude, we found that the amplitude of the induced parallel flows has a parabolic radial structure. It is not a surprise, as the amplitude of the parallel motions is proportional to the mother torsional wave amplitude squared: the parallel flows could not be nonlinearly induced near the flux tube axis, where the mother wave amplitude tends to zero. This result is different from the flat radial dependence assumed in the thin flux tube approximation given by expressions (A1). However, it does not show a problem with the thin flux tube approximation, as there the physical quantities are taken either at the flux tube axis or its boundary. The empirically determined best-fitting dependences of the radial profiles of the velocity vector components could be of interest for forward modelling of tor-

sional waves, e.g. in the further development of the studies of Van Doorsselaere et al. (2016).

Our study demonstrates the importance of the transverse profile for the evolution of coronal torsional waves. The follow-up work should account important effects of stratification, and the variation of the flux tube area and plasma temperature.

5. ACKNOWLEDGEMENTS

APPENDIX

A. WEAKLY NONLINEAR TORSIONAL WAVES IN THIN FLUX TUBE APPROXIMATION

We illustrate the excitation of compressive perturbations by the analysis of long-wavelength weakly nonlinear torsional Alfvén waves. Consider perturbations of a straight cylindrical magnetic flux tube, using the cylindrical coordinate axis with the axis z coinciding with the flux tube's axis. A torsional Alfvén wave consists of alternate twisting azimuthal motions v_φ of the plasma, accompanied by the azimuthal components of the magnetic field B_φ. Since both quantities should vanish on the axis of the magnetic tube, torsional Alfvén waves could be considered in terms of the second order thin flux-tube approximation of Zhugzhda (1996). In this approach, the parallel wavelength of the perturbations is taken to be much larger than the flux tube radius, which allows one to consider only a few lowest order terms in the Taylor expansion with respect to the radial coordinate,

$$\rho \approx \tilde{\rho}, \ p \approx \tilde{p} + p_2 r^2, \ v_r \approx Vr, \ v_\varphi \approx \Omega r, \ v_z \approx u$$
$$B_r \approx B_{r1} r, \ B_\varphi \approx Jr, \ B_z \approx \widetilde{B_z} + B_{z2} r^2, \tag{A1}$$

where B_r, B_φ, and B_z are the radial, azimuthal and longitudinal components of the magnetic field, and v_r, v_φ, and v_z are the radial, azimuthal and parallel components of the velocity, respectively; V, Ω and J are the radial derivates of the radial and azimuthal components of the velocity, and the azimuthal field, respectively; ρ is the mass density; and p is the gas pressure. The quantities with the overtilde are the zeroth order terms of the expansions with respect to the radial coordinate. The overtilde will be omitted hereafter. In the derivation of these equations it is assumed that the longitudinal wavelength of the perturbations is much larger than the radius of the flux tube.

Applying expansion (A1) to the ideal MHD equations, and omitting terms with higher degrees of r, one obtains

$$\rho\left(\frac{\partial V}{\partial t} + u\frac{\partial V}{\partial z} + V^2 - \Omega^2\right) + 2p_2 + \frac{1}{2\pi}\left(J^2 + B_z B_{z2}\right) - \frac{1}{4\pi}B_z\frac{\partial B_{r1}}{\partial z} = 0, \tag{A2}$$

$$\frac{\partial \Omega}{\partial t} + u\frac{\partial \Omega}{\partial z} + 2V\Omega + \frac{J}{4\pi\rho}\frac{\partial B_z}{\partial z} - \frac{B_z}{4\pi\rho}\frac{\partial J}{\partial z} = 0, \tag{A3}$$

$$\rho\left(\frac{\partial u}{\partial t} + u\frac{\partial u}{\partial z}\right) + \frac{dp}{dz} = 0, \tag{A4}$$

$$\frac{\partial \rho}{\partial t} + \frac{\partial(\rho u)}{\partial z} + 2\rho V = 0, \tag{A5}$$

$$\frac{\partial B_{r1}}{\partial t} + \frac{\partial(u B_{r1})}{\partial z} - \frac{\partial(V B_z)}{\partial z} = 0, \tag{A6}$$

$$\frac{\partial J}{\partial t} + \frac{\partial(uJ)}{\partial z} - \frac{\partial \Omega B_z}{\partial z} + 2VJ - 2\Omega B_{r1} = 0, \tag{A7}$$

$$\frac{\partial B_z}{\partial t} + u\frac{\partial B_z}{\partial t} + 2B_z V = 0, \tag{A8}$$

$$\left(\frac{\partial}{\partial t} + u\frac{\partial}{\partial z}\right)\frac{p}{\rho^\gamma} = 0, \tag{A9}$$

$$2B_{r1} + \frac{\partial B_z}{\partial z} = 0. \tag{A10}$$

The effect of the gravitational force is neglected. All considered physical parameters are independent of the azimuthal coordinate, i.e. $\partial/\partial\varphi = 0$. In other words, we restrict our attention to the consideration of the axisymmetric perturbations only.

The equations are supplemented by the magnetic flux conservation equation and total pressure balance at the tube boundary,

$$B_z A = const, \tag{A11}$$

$$p + \frac{B_z^2}{8\pi} - \frac{A}{2\pi}\left[\rho\left(\frac{\partial V}{\partial t} + u\frac{\partial V}{\partial z} + V^2 - \Omega^2\right) + \frac{1}{4\pi}\left(J^2 - \frac{1}{4}\left(\frac{\partial B_z}{\partial z}\right)^2 + \frac{B_z}{2}\frac{\partial^2 B_z}{\partial z^2}\right)\right] = p_T^{\text{ext}}, \tag{A12}$$

where $A = \pi R^2$ is the cross-sectional area of the tube of radius R, and p_T^{ext} is the external total pressure.

The equations are linearised with respect to the equilibrium that is an untwisted and non-rotating flux tube, ρ_0, p_0, B_{z0}, A_0 (or R_0), and $u_0 = V_0 = J_0 = \Omega_0 = B_{r1}^0 = 0$. All equilibrium quantities are constant.

In the linear regime, torsional motions are decoupled from compressible motions. Torsional perturbations given by Ω and J and described by Eqs. (A3) and (A7),

$$\frac{\partial\Omega}{\partial t} - \frac{B_{z0}}{4\pi\rho_0}\frac{\partial J}{\partial z} = 0, \tag{A13}$$

$$\frac{\partial J}{\partial t} - B_{z0}\frac{\partial\Omega}{\partial z} = 0, \tag{A14}$$

which are readily combined in the wave equation

$$\frac{\partial^2 J}{\partial t^2} - C_A^2\frac{\partial^2 J}{\partial z^2} = 0, \tag{A15}$$

where $\omega/k = C_A$ and $C_A = B_{z0}/\sqrt{4\pi\rho_0}$ is the Alfvén speed. A harmonic torsional wave is $J = J_M\cos(\omega t - kz)$ and $\Omega = \Omega_M\cos(\omega t - kz)$, where the constant amplitudes $\Omega_M = -J_M/\sqrt{4\pi\rho_0}$.

Compressive perturbations given by u, V, ρ, p, B_z, A, and linked by Eqs. (A4), (A5), (A8), (A9), (A11) and (A12). Excluding all variables but u, one can readily obtain the wave equation

$$\frac{\partial^2 u}{\partial t^2} - C_T^2\frac{\partial^2 u}{\partial z^2} = 0 \tag{A16}$$

where $C_T = C_A C_S/(C_A^2 + C_S^2)^{1/2}$ is the tube speed, and $C_S = \sqrt{\gamma p_0/\rho_0}$ is the sound speed. Equation (A16) has a propagating wave solution $u = U_m\cos(\omega t - kz)$, where U_m is a constant amplitude, and $\omega/k = C_T$.

Consider nonlinear interaction of torsional and compressible waves of finite amplitudes. Taking into account the quadratically nonlinear term containing the torsional variables in the derivation of Eq. (A16), we obtain the inhomogeneous wave equation

$$\frac{\partial^2 u}{\partial t^2} - C_T^2\frac{\partial^2 u}{\partial z^2} = -\frac{R_0^2 C_T^2}{4\pi\rho_0 C_S^2}\frac{\partial}{\partial t}\left(J\frac{\partial J}{\partial z}\right). \tag{A17}$$

The right hand side term of Eq. (A17) describes the ponderomotive force. The solution of the equation is a sum of solutions of the homogeneous and inhomogeneous equations, i.e. the longitudinal, or "tube" wave propagating at the tube speed, C_T, and the induced, "ponderomotive" wave propagating at C_A. The ponderomotive wave constitutes the Alfvénic wind.

If the torsional wave is driven by a harmonic oscillation with the frequency ω at a certain location $z = 0$, the solution of the equation is:

$$u = \begin{cases} u_T + u_p, & 0 < z < C_T t, \\ u_p, & C_T t < z < C_A t, \\ 0, & z > C_A t, \end{cases} \tag{A18}$$

where the tube wave $u_T(z, t)$ is

$$u_T = \frac{R_0^2 J_M^2}{16\pi\rho_0 C_A}\{\cos[2\omega(t - z/C_T)] - 1\} = \frac{R_0^2\Omega_M^2}{4C_A}\{\cos[2\omega(t - z/C_T)] - 1\}, \tag{A19}$$

and the ponderomotive wave $u_p(z, t)$ is

$$u_p = \frac{R_0^2 J_M^2}{16\pi\rho_0 C_A}\{1 - \cos[2\omega(t - z/C_A)]\} = \frac{R_0^2\Omega_M^2}{4C_A}\{1 - \cos[2\omega(t - z/C_A)]\}. \tag{A20}$$

Equation (A18) indicates that in the weakly nonlinear case, torsional Alfvén wave induces parallel flows that consist of two motions, the tube wave u_T and the ponderomotive wave u_p, both of which have the amplitude $R_0^2 \Omega_M^2 / 4 C_A$ and the frequency that is double the driving frequency. These parallel flows are accompanied by the perturbations of the plasma density ρ. Hence the nonlinearly induced perturbations are compressive.

However, this formalism does not allow one to take into account the effect of nonlinear phase mixing, connected with the increasing non-uniformity of the torsional wave fronts across the equilibrium magnetic field.

B. WEAKLY NONLINEAR EFFECTS ASSOCIATED WITH ALFVÉN WAVE PHASE MIXING

Consider a plane Alfvén wave in a plasma with a 1D non-uniformity of the Alfvén speed across the field. For simplicity the plasma is taken to be of zero-β. In this consideration we follow the formalism developed in (Botha et al. 2000). Let the equilibrium magnetic field of the strength B_0 be directed along the z-axis. The equilibrium density of the plasma, ρ_0, varies in the x-direction. A linearly polarised Alfvén wave is characterised by the perturbations of B_y and V_y.

In the weakly nonlinear case we can restrict our attention to the quadratically nonlinear terms only. In this case, the nonlinearly induced flows are described by the equations

$$\frac{\partial^2 V_z}{\partial t^2} = -\frac{1}{\rho_0} \left[\frac{\partial}{\partial t} \left(B_y \frac{\partial B_y}{\partial z} \right) \right], \tag{B21}$$

$$\frac{\partial^2 V_x}{\partial t^2} - C_A^2(x) \left(\frac{\partial^2 V_x}{\partial x^2} + \frac{\partial^2 V_x}{\partial z^2} \right) = -\frac{1}{\rho_0} \left[\frac{\partial}{\partial t} \left(B_y \frac{\partial B_y}{\partial x} \right) \right]. \tag{B22}$$

Both these flows are essentially compressive, as both cause the density perturbation,

$$\rho = - \int \left[\frac{\partial}{\partial x} (\rho_0 V_x) + \frac{\partial}{\partial z} (\rho_0 V_z) \right] dt. \tag{B23}$$

Equation (B21) is similar to Equation (A17), in the zero-β limit. It describes the nonlinear excitation of the parallel plasma flows by the Alfvén wave, the ponderomotive wave or the Alfvénic wind. It is clear that the induced parallel flows have the highest speed at the magnetic field lines where the amplitude of the Alfvén wave is the highest.

Equation (B22) that describes the nonlinearly induced perpendicular flows is essentially different. Its left hand side describes freely propagating fast magnetoacoustic waves that are subject to refraction connected with the non-uniformity of $C_A(x)$. In particular, in a magnetic flux tube with the enhanced plasma density, this effect leads to the appearance of fast magnetoacoustic modes, for example, sausage modes (e.g. Nakariakov et al. 2012). The nonlinear excitation of the perpendicular compressive flows occurs when the Alfvén wave is non-uniform in the perpendicular direction. Because of Alfvén wave phase mixing, the right hand side term experiences continuous growth, magnifying the effect of the nonlinear excitation.

REFERENCES

Alfvén, H. 1942, Nature, 150, 405

Antolin, P., & Shibata, K. 2010, ApJ, 712, 494

Bisnovatyi-Kogan, G. S. 2007, Monthly Notices of the Royal Astronomical Society, 376, 457

Botha, G. J. J., Arber, T. D., Nakariakov, V. M., & Keenan, F. P. 2000, Astronomy & Astrophysics, 363, 1186

Charbonneau, P., & MacGregor, K. B. 1995, ApJ, 454, 901

Chaston, C. C., Carlson, C. W., Ergun, R. E., & McFadden, J. P. 2000, Physica Scripta, 2000, 64

Cheng, C., Chen, L., & Chance, M. 1985, Annals of Physics, 161, 21

Childs, H., Brugger, E., Whitlock, B., et al. 2012, in High Performance Visualization–Enabling Extreme-Scale Scientific Insight, 357–372

Cohen, R. H., & Kulsrud, R. M. 1974, Physics of Fluids, 17, 2215

Cooper, F. C., Nakariakov, V. M., & Williams, D. R. 2003, A&A, 409, 325

Copil, P., Voitenko, Y., & Goossens, M. 2008, A&A, 478, 921

Cranmer, S. R. 2009, Living Reviews in Solar Physics, 6, 3

Edwin, P. M., & Roberts, B. 1983, SoPh, 88, 179

Fedun, V., Verth, G., Jess, D. B., & Erdélyi, R. 2011, The Astrophysical Journal, 740, L46

Fletcher, L., & Hudson, H. S. 2008, ApJ, 675, 1645

Heyvaerts, J., & Priest, E. R. 1983, Astronomy & Astrophysics, 117, 220

Hollweg, J. V. 1971, J. Geophys. Res., 76, 5155

Hood, A. W., Brooks, S. J., & Wright, A. N. 2002, Proceedings of the Royal Society of London Series A, 458, 2307

Kudoh, T., & Shibata, K. 1999, ApJ, 514, 493

Laming, J. M. 2015, Living Reviews in Solar Physics, 12, 2

Malara, F., Primavera, L., & Veltri, P. 1996, ApJ, 459, 347

Matsumoto, T., & Suzuki, T. K. 2012, ApJ, 749, 8

McLaughlin, J. A., De Moortel, I., & Hood, A. W. 2011, Astronomy & Astrophysics, 527, A149

Mikhalyaev, B. B., & Bembitov, D. B. 2014, SoPh, 289, 4069

Murawski, K., Solov'ev, A., Musielak, Z. E., Srivastava, A. K., & Kraśkiewicz, J. 2015, A&A, 577, A126

Nakariakov, V. M., Hornsey, C., & Melnikov, V. F. 2012, ApJ, 761, 134

Nakariakov, V. M., Ofman, L., & Arber, T. D. 2000, A&A, 353, 741

Nakariakov, V. M., Roberts, B., & Murawski, K. 1997, Solar Physics, 175, 93

Nakariakov, V. M., Roberts, B., & Murawski, K. 1998, A&A, 332, 795

Ofman, L., & Davila, J. M. 1995, J. Geophys. Res., 100, 23413

—. 1998, J. Geophys. Res., 103, 23677

Poedts, S., & Boynton, G. C. 1996, A&A, 306, 610

Porth, O., Xia, C., Hendrix, T., Moschou, S. P., & Keppens, R. 2014, ApJS, 214, 4

Ruderman, M. S. 1999, ApJ, 521, 851

Ruderman, M. S., Berghmans, D., Goossens, M., & Poedts, S. 1997, A&A, 320, 305

Sadovnichy, V., Tikhonravov, A., Voevodin, V., & Opanasenko, V. 2013, Contemporary High Performance Computing: From Petascale toward Exascale (Chapman & Hall/CRC Computational Science), ed. J. S. Vetter (Boca Raton, USA, CRC Press, 2013), 283–307

Shestov, S., Nakariakov, V. M., & Kuzin, S. 2015, The Astrophysical Journal, 814, 135

Srivastava, A. K., Shetye, J., Murawski, K., et al. 2017, Scientific Reports, 7, 43147

Suzuki, T. K. 2011, SSRv, 158, 339

Tikhonchuk, V. T., Rankin, R., Frycz, P., & Samson, J. C. 1995, Physics of Plasmas, 2, 501

Tsiklauri, D., & Nakariakov, V. M. 2002, A&A, 393, 321

Tsiklauri, D., Nakariakov, V. M., & Rowlands, G. 2003, A&A, 400, 1051

Uberoi, C. 1995, Physica Scripta Volume T, 60, 20

Van Doorsselaere, T., Antolin, P., Yuan, D., Reznikova, V., & Magyar, N. 2016, Frontiers in Astronomy and Space Sciences, 3, 4

Van Doorsselaere, T., Nakariakov, V. M., & Verwichte, E. 2008, ApJL, 676, L73

Vasheghani Farahani, S., Nakariakov, V. M., Van Doorsselaere, T., & Verwichte, E. 2011, Astronomy & Astrophysics, 526, A80

Vasheghani Farahani, S., Nakariakov, V. M., Verwichte, E., & Van Doorsselaere, T. 2012, Astronomy & Astrophysics, 544, A127

Williams, T., Taroyan, Y., & Fedun, V. 2016, ApJ, 817, 92

Wójcik, D., Murawski, K., Musielak, Z. E., Konkol, P., & Mignone, A. 2017, SoPh, 292, 31

Yu, H., Li, B., Chen, S.-X., Xiong, M., & Guo, M.-Z. 2016, ApJ, 833, 51

Zheng, J., Chen, Y., & Yu, M. 2016, Phys. Scr., 91, 015601

Zhugzhda, Y. D. 1996, Physics of Plasmas, 3, 10